Analysis of Pulse Width Modulation Methods for PMSM Sensorless Control Based on Current Derivative Measurement

Gyu Cheol Lim, Juwon Lee, Byung Ryang Park, and Jung-Ik Ha
Department of Electrical and Computer Engineering Seoul National University, Seoul, Korea

***Abstract*--For a full-region sensorless control based on the current derivative, modifying the pulse-width modulation (PWM) eliminates the dead zone at a low modulation index (MI). This paper proposes and analyzes the various PWM methods for the full-region sensorless control of permanent magnet synchronous motor (PMSM). The position estimation error is extracted from the current derivative in one active voltage vector (AVV), and the actual rotor position is obtained using a Luenberger observer. To achieve a sufficient AVV for current derivative measurement, four types of PWM methods are introduced. The performance of each PWM method is analyzed and compared in terms of the motor drive and position estimation. In addition, the implementation of each PWM using the digital signal processor (DSP) is explained, and the compensation methods are applied to improve the drive performance. The effectiveness of the proposed method is verified by a 1 kW PMSM drive system, and the results show that the rotor position is accurately estimated within an error of less than 0.2 rad.**

***Index Terms* — Current Derivative measurement, pulse width modulation, sensorless drive .**

I. Introduction

To reduce the high cost and size of the position sensor, the position sensorless control of the permanent magnet synchronous motor (PMSM) has been studied in past decades [1]. Significantly, the fundamental pulse-width modulation (PWM) based sensorless control method is getting attention for a full-region sensorless control [2]-[3]. Using the PWM based method, the rotor position is estimated using the value of the current derivative at a certain voltage vector, while no additional filters are required for the signal processing [4].

Due to the parasitic components of the motor driving system, an oscillation of the phase current occurs at a switching instants [5]. As the current oscillation is detrimental to an accurate measurement of the current derivative, the phase current is sampled a little after the switching instant. Accordingly, the duration of the voltage vector for the current derivative measurement needs to be secured sufficiently. However, in the conventional PWM methods, the duration of the voltage vector is not secured at a certain operating point, and therefore the sensorless control is not applicable. The previous research tried to overcome this issue by modifying the fundamental PWM [6]-[13]. In [6], the measurement vector was inserted between the fundamental PWM sequence, while the discontinuous PWM was utilized. Meanwhile, the current derivative was measured in three voltage vectors among the PWM sequence, while the space vector PWM (SVPWM) was modified and an asymmetric PWM method was applied for the sensorless control [7]-[9]. Moreover, a method combining the modified PWM and the conventional SVPWM according to the modulation index (MI) was proposed [10]. In [11], the multi-SVPWM based sensorless control method was proposed, where the six active voltage vectors were all utilized. Also, the asymmetric and symmetric PWM methods using the four active voltage vectors for the sensorless control were proposed [12]-[13].

In this paper, the PWM methods for the PMSM sensorless control are proposed, analyzed, and compared. The sensorless control method proposed in the previous research is introduced [13]-[14], and the dead zone is analyzed when the conventional PWM is utilized. Then, various PWM methods such as R3PWM, R4PWM, and T4PWM are proposed, which effectively eliminate the sensorless dead zone of the conventional PWM. Moreover, the proposed PWM methods are analyzed in terms of the motor drive and position estimation performance. The carrier-based implementation of each PWM and its practical issue is explained. At last, the proposed PWM methods are validated by the experimental results of a 1 kW PMSM sensorless control.

II. Sensorless Control Method of PMSM Based on Current Derivative

A. Position sensorless control algorithms

The position estimation method employs a rotor field-oriented (RFO) reference frame f^r_{dq} and an estimated field-oriented (EFO) reference frame $\hat{f}^r_{dq}$, as shown in Fig. 1. The error of the actual and estimated position and speed, and the transformation matrix between the reference frame are expressed as

$$\tilde{\theta}_r = \theta_r - \hat{\theta}_r, \tilde{\omega}_r = \omega_r - \hat{\omega}_r \quad (1)$$

$$R(\tilde{\theta}_r) = \begin{bmatrix} \cos(\tilde{\theta}_r) & \sin(\tilde{\theta}_r) \\ -\sin(\tilde{\theta}_r) & \cos(\tilde{\theta}_r) \end{bmatrix}$$
$$f_{dq}^r = R(\tilde{\theta}_r)\hat{f}_{dq}^r \tag{2}$$

while the coordinate transform of voltage, current, and current derivative is derived as

$$\begin{bmatrix} v_{ds}^r \\ v_{qs}^r \end{bmatrix} = R(\tilde{\theta}_r)\begin{bmatrix} \hat{v}_{ds}^r \\ \hat{v}_{qs}^r \end{bmatrix}$$
$$\begin{bmatrix} i_{ds}^r \\ i_{qs}^r \end{bmatrix} = R(\tilde{\theta}_r)\begin{bmatrix} \hat{i}_{ds}^r \\ \hat{i}_{qs}^r \end{bmatrix} \tag{3}$$
$$\frac{d}{dt}\begin{bmatrix} i_{ds}^r \\ i_{qs}^r \end{bmatrix} = R(\tilde{\theta}_r)\frac{d}{dt}\begin{bmatrix} \hat{i}_{ds}^r \\ \hat{i}_{qs}^r \end{bmatrix} + \frac{d}{dt}R(\tilde{\theta}_r)\begin{bmatrix} \hat{i}_{ds}^r \\ \hat{i}_{qs}^r \end{bmatrix}.$$

Meanwhile, the motor equation of PMSM using the RFO reference frame is expressed as

$$\begin{bmatrix} v_{ds}^r \\ v_{qs}^r \end{bmatrix} = R_s\begin{bmatrix} i_{ds}^r \\ i_{qs}^r \end{bmatrix} + \begin{bmatrix} L_d & 0 \\ 0 & L_q \end{bmatrix}\frac{d}{dt}\begin{bmatrix} i_{ds}^r \\ i_{qs}^r \end{bmatrix} + \omega_r\begin{bmatrix} 0 & -L_q \\ L_d & 0 \end{bmatrix}\begin{bmatrix} i_{ds}^r \\ i_{qs}^r \end{bmatrix} + \omega_r\begin{bmatrix} 0 \\ \lambda_f \end{bmatrix}. \tag{4}$$

Using (3) and (4), the pre-presented research derived the estimated position value [13]. Assuming the speed error is sufficiently small, the difference between the actual and estimated position is derived as

$$\tilde{\theta}_r = \operatorname{atan}\left(\frac{\frac{d}{dt}\hat{i}_{ds}^r - \frac{1}{L_d}\hat{v}_{ds}^r + \frac{R_s}{L_d}\hat{i}_{ds}^r - \hat{\omega}_r\frac{L_q}{L_d}\hat{i}_{qs}^r}{-\frac{d}{dt}\hat{i}_{qs}^r + \frac{1}{L_d}\hat{v}_{qs}^r - \hat{\omega}_r\frac{L_q}{L_d}\hat{i}_{ds}^r - \frac{R_s}{L_d}\hat{i}_{qs}^r}\right). \tag{5}$$

Noticeably, the estimation error $\tilde{\theta}_r$ is expressed only in the EFO reference frame, which only requires the estimated position. In addition, all the terms in (0) are the instantaneous values of voltage, current, and current derivative. Accordingly, the sampling of the phase current is required in only one active voltage vector.

For a closed-loop estimation, the actual rotor position is derived from the position error using the third-order Luenberger observer as described in Fig. 2. The state equation of the observer is expressed as

$$\frac{\hat{\theta}_r}{\theta_r} = \frac{Js^3 + (B + \hat{J}L_1)s^2 + (\hat{B}L_1 + L_2)s + L_3}{\hat{J}s^3 + (\hat{B} + \hat{J}L_1)s^2 + (\hat{B}L_1 + L_2)s + L_3} \tag{6}$$

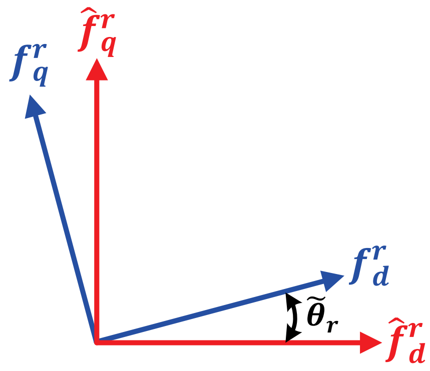

Fig. 1. Diagram of the rotor field-oriented reference frame (blue) and estimated field-oriented reference frame (red).

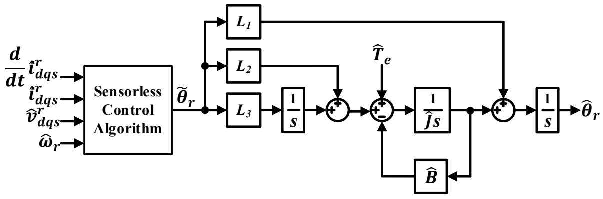

Fig. 2. Block diagram of closed-loop estimation using the sensorless control algorithm and third-order Luenberger observer.

where J, B each refers to the inertia and viscous damping of the machine and $L_{1\sim3}$ refers to the observer gain.

B. Current derivative measurement

For an accurate measurement of the current derivative, the multi-point current sampling (MPCS) is utilized, which is robust to the measurement error. Meanwhile, the phase current is sampled later than the switching instant by the current oscillation time. Therefore, the duration of the current sampling voltage vector (CSVV), t_{csvv}, has to be longer than the sum of the oscillation time t_{osc}, the analog-to-digital conversion (ADC) time t_{adc} for the current sensing and the dead time t_{dead} of power switches, which is expressed as

$$t_{CSVV} \geq t_{osc} + N_s t_{adc} + t_{dead} = t_{min}. \tag{7}$$

N_s indicates the number of the current sampling, which is determined by the computing time of the control system. Using the sensorless control algorithm, only one CSVV is selected between the fundamental PWM sequence and is required to satisfy the minimum time in (0), which reduces the constraints on the modulation method.

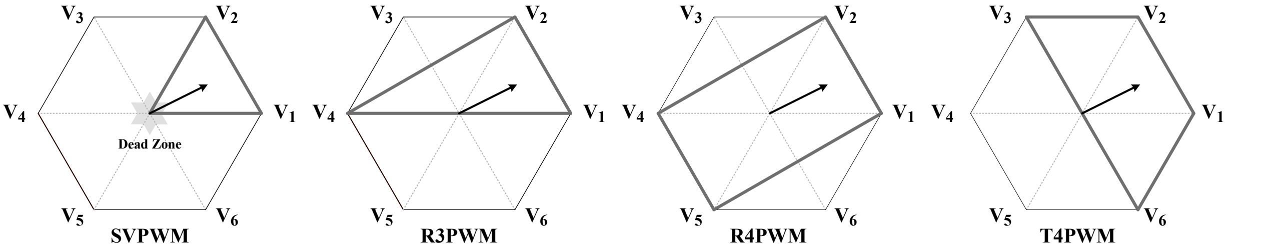

Fig. 3. Proposed PWM methods and sensorless dead zone at a low MI.

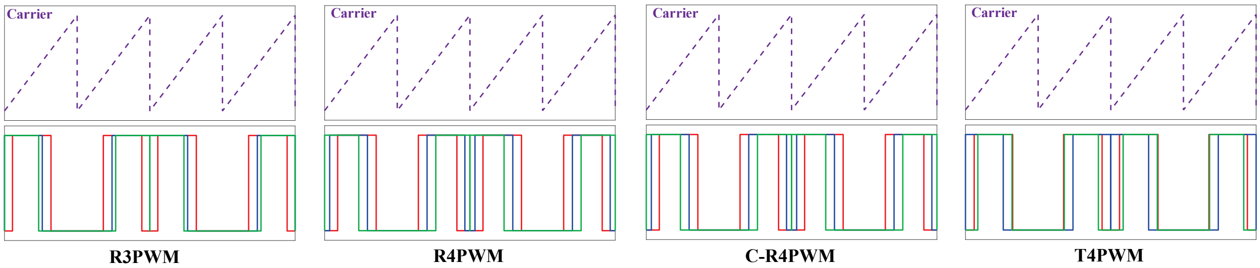

Fig. 4. Switching state of each PWM method at the space vector region in Fig. 3.

III. Analysis of PWM Methods for Sensorless Control

A. *Deadzone analysis and modified PWM for sensorless control*

Since the conventional SVPWM is advantageous for the DC-link voltage utilization, it is widely used for various PMSM drive applications. However, at a low MI condition, the zero voltage vector (ZVV) accounts for most of the switching state [2]. Thus, an operating point exists where the active voltage vector (AVV) does not satisfy the condition (0), and the sensorless control is not applicable. The dead zone of sensorless control using SVPWM is described in Fig. 3.

In order to eliminate the dead zone, various PWM methods are proposed as shown in Fig. 3. The first one is a right-angled triangular PWM (R3PWM), where the duration of the shortest AVV, which does not meet (0), is lengthened. To synthesize the fundamental voltage, the complementary voltage vector of the shortest AVV is added. The next one is a rectangular PWM (R4PWM), where all the AVVs not satisfying (0) is lengthened. To synthesize the fundamental voltage, the complementary voltage vectors of all the stretched AVVs are added. Moreover, the voltage of which MI is lower than 0.577 is able to be synthesized using the four rectangular AVVs without rotating the rectangle according to the space vector region. The PWM using the rotating rectangle is called R4PWM, while the PWM using the constant rectangle is called constant-R4PWM (C-R4PWM). While the R3PWM and R4PWM lengthen the AVVs, the trapezoidal PWM (T4PWM) does not modify the AVVs but substitutes the part of ZVVs with two complementary AVVs. The duration of the additional AVV is set according to the condition (0) and is utilized for the CSVV.

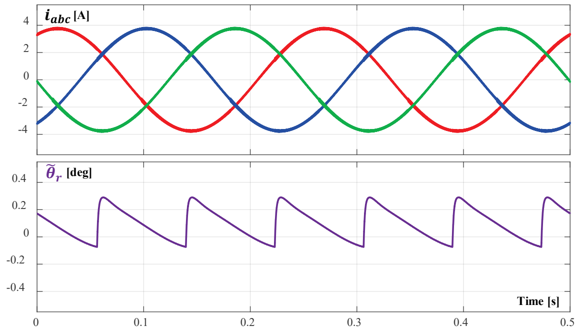

Fig. 5. Block diagram of closed-loop estimation using the sensorless control algorithm and third-order Luenberger observer.

TABLE I
Performance Analysis of PWM Methods

PWM Methods	THD of Phase Current [%]	Position Estimation Error RMS [°]
R3PWM	1.14	0.18
R4PWM	1.40	0.14
C-R4PWM	2.07	2.66
T4PWM	1.62	2.56

Fig. 4 shows the sawtooth-shaped carrier function and the switching state of each PWM method at the space vector region described in Fig. 3. For an average current sampling, the PWM occurs symmetrically. Moreover, the phase current derivative is measured at the CSVV in each PWM and utilized for the position sensorless control.

B. *Performance analysis of PWM methods*

To evaluate the PWM methods for the PMSM sensorless control, two types of performance index are introduced: drive index (DI) and estimation index (EI). DI indicates the impact of the PWM in terms of the motor driving, such as the total harmonic distortion (THD) of the phase current and the effect of the dead time on the voltage synthesizing. EI indicates the effectiveness of the position estimation using each PWM method. The performance analysis of the PWM is conducted by the PLECS simulation results, as described in Fig. 5 and Table I. The THD of the phase current is related to the output torque ripple and loss in the motor drive system. The R3PWM has the least current THD, since the additional AVV is minimized among the PWM methods. Meanwhile, the RMS of position estimation error is minimized in R4PWM, since the transition of the CSVV is the least.

IV. Experimental Results

The overall block diagram of the proposed PWM based sensorless control is shown in Fig. 6. In the digital signal processor (DSP), the MPCS of the phase current is performed using the ADC peripheral, the estimated rotor position is extracted by the sensorless algorithm and observer, and the modified PWM signal is produced using the PWM peripheral.

The experiment setup is described in Fig. 7, and the parameters of the driving system and target PMSM are listed in Table II. Fig. 8 and 9 show a part of the simulation and experimental results of the proposed PWM based sensorless control. The R3PWM method is applied at a low MI with a rated load in Fig. 8. The position estimation error is within 0.01 rad at the steady-state operation and within 0.03 rad at the dynamic operation. Also, the T4PWM method is implemented using DSP and applied at a low MI with a rated load in Fig. 9. The position estimation error is within 0.1 rad at the steady-state operation and within 0.2 rad at the dynamic operation. The results represent that the proposed PWM based sensorless control is effective in various driving conditions.

V. Conclusion

In this paper, the PWM methods for the PMSM sensorless control are introduced. For a full-region sensorless control, the fundamental PWM sequence is modified by securing the sufficient duration of CSVV. The performance of R3PWM, R4PWM, C-R4PWM, and T4PWM is analyzed and compared in terms of the sensorless control. The proposed PWM methods are implemented using DSP and are verified by the 1 kW PMSM drive system.

TABLE II
Parameters of Target PMSM

Symbol	Parameter	Nominal Value
P	Pole	8
V_{dc}	DC Link Voltage	**150 V**
$T_{e,rated}$	Rated Torque	**6.4 Nm**
P_{rated}	Rated Power	**1 kW**
R_s	Stator Resistance	**0.9 Ω**
L_d	D-axis Inductance	**9.4 mH**
L_q	Q-axis Inductance	**18.1 mH**
λ_f	Flux Linkage	**183 mV·s**

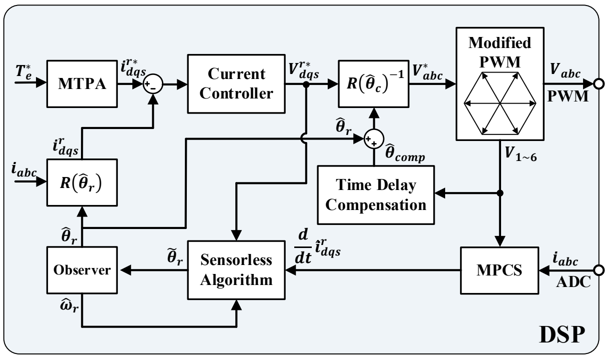

Fig. 6. Block diagram of proposed PWM based sensorless control.

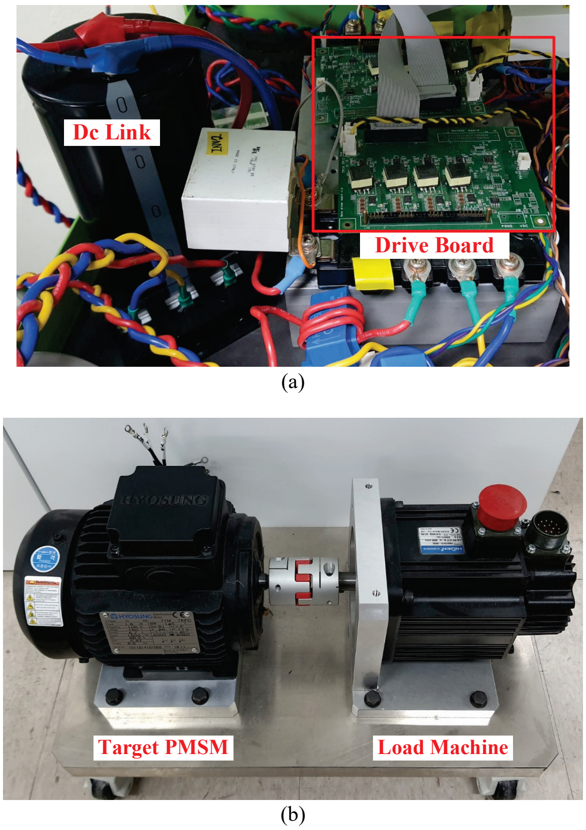

Fig. 7. (a) Motor drive system (b) Target PMSM and load machine.

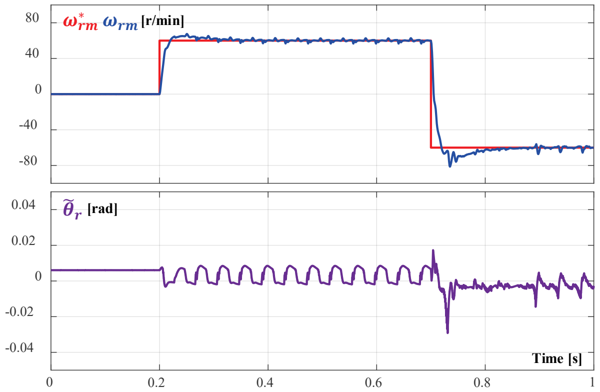

Fig. 8. Simulation result of sensorless drive with varying speed codition: $\omega_{rm} = -60$ to 60 r/min, $T_e = 1$ p. u., using R3PWM.

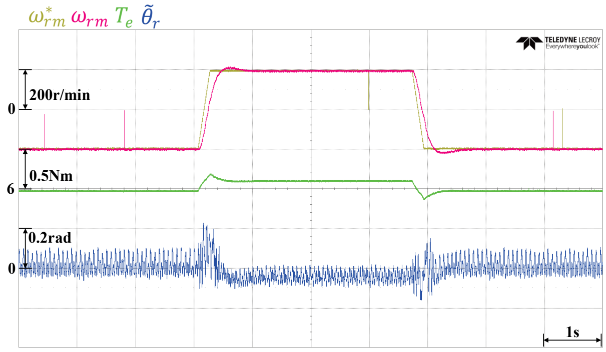

Fig. 9. Experimental result of sensorless drive with varying speed condition: $\omega_{rm} = -200$ to 200 r/min, $T_e = 1$ p. u., using T4PWM.

REFERENCES

[1] G. Wang, M. Valla, and J. Solsona, "Position Sensorless Permanent Magnet Synchronous Machine Drives—A Review," *IEEE Transactions on Industrial Electronics*, vol. 67, no. 7, pp. 5830-5842, 2020.

[2] Q. Gao, G. M. Asher, M. Sumner, and P. Makys, "Position Estimation of AC Machines Over a Wide Frequency Range Based on Space Vector PWM Excitation," *IEEE Transactions on Industry Applications*, vol. 43, no. 4, pp. 1001-1011, 2007.

[3] M. X. Bui, M. F. Rahman, and D. Xiao, "A Hybrid Sensorless Controller of an Interior Permanent Magnet Synchronous Machine Using Current Derivative Measurements and a Sliding Mode Observer," *IEEE Transactions on Industry Applications*, vol. 56, no. 1, pp. 314-324, 2020.

[4] S. Jung and J.-I. Ha, "Analog Filtering Method for Sensorless AC Machine Control With Carrier-Frequency Signal Injection," *IEEE Transactions on Industrial Electronics*, vol. 62, no. 9, pp. 5348-5358, 2015.

[5] A. E. Ginart, D. W. Brown, P. W. Kalgren, and M. J. Roemer, "Online Ringing Characterization as a Diagnostic Technique for IGBTs in Power Drives," *IEEE Transactions on Instrumentation and Measurement*, vol. 58, no. 7, pp. 2290-2299, 2009.

[6] J.-Y. Chen, K.-Y. Hung, G.-R. Chen, and S.-C. Yang, "Integration of Measurement Vector Insertion With Discontinuous PWM to Improve Saliency-Based Sensorless Drive Position Estimation," *IEEE Transactions on Power Electronics*, vol. 37, no. 12, pp. 15283-15296, 2022.

[7] C. Wu, Z. Chen, and Q. Chen, "An Optimized Asymmetric Pulsewidth Modulation for Sensorless Control of Permanent Magnet Synchronous Machines," *IEEE Transactions on Industrial Electronics*, vol. 69, no. 2, pp. 1389-1399, 2022.

[8] M. S. Mubarok and T.-H. Liu, "An Adjustable Wide-Range Speed-Control Method for Sensorless IPMSM Drive Systems," *IEEE Access*, vol. 10, pp. 42727-42738, 2022.

[9] J.-Y. Chen and S.-C. Yang, "Saliency-Based Permanent Magnet Machine Position Sensorless Drive Using Proposed PWM Injection and Shunt-Based Current Sensing for Position Estimation," *IEEE Transactions on Industrial Electronics*, vol. 68, no. 7, pp. 5693-5703, 2021.

[10] C. Wu, Z. Chen, and Q. Chen, "Hybrid-Modulation-Based Full-Speed Sensorless Control for Permanent Magnet Synchronous Motors," *IEEE Transactions on Power Electronics*, vol. 37, no. 5, pp. 5908-5917, 2022.

[11] M. Gu, S. Ogasawara, and M. Takemoto, "Novel PWM Schemes With Multi SVPWM of Sensorless IPMSM Drives for Reducing Current Ripple," *IEEE Transactions on Power Electronics*, vol. 31, no. 9, pp. 6461-6475, 2016.

[12] X. Luo, Q. Tang, A. Shen, H. Shen, and J. Xu, "A Combining FPE and Additional Test Vectors Hybrid Strategy for IPMSM Sensorless Control," *IEEE Transactions on Power Electronics*, vol. 33, no. 7, pp. 6104-6113, 2018.

[13] J. Lee, B. R. Park, G. C. Lim and J. -I. Ha, "Hybrid Pulse Width Modulation with Current Derivative Measurement for PMSM Sensorless Control," 2023 *IEEE Applied Power Electronics Conference and Exposition (APEC)*, Orlando, FL, USA, 2023, pp. 1090-1096, doi: 10.1109/APEC43580.2023.10131520.

[14] B. R. Park, G. C. Lim, Y. Han and J. -I. Ha, "Saliency-Based Sensorless Control Using Current Derivative in IPMSM Drives With Single DC-Link Current Sensor," in *IEEE Transactions on Industrial Electronics*, doi: 10.1109/TIE.2023.3274858.